J. Phys. Chem. B **2001,** *105,* 6211−6220

Supported Tantalum Oxide and Supported Vanadia-tantala Mixed Oxides: Structural Characterization and Surface Properties

Michael Baltes,*,† Arla Kytökivi,‡ Bert M. Weckhuysen,§ Robert A. Schoonheydt,‖
Pascal Van Der Voort,† and Etienne F. Vansant†

Laboratory of Adsorption and Catalysis, Department of Chemistry, University of Antwerpen (U.I.A.),
Universiteitsplein 1, 2610 Wilrijk, Belgium, Fortum Oil and Gas Oy, Oil, Research and Development,
POB 110, 00048 Fortum, Keilaranta 6, Espoo, Finland, Department of Inorganic Chemistry and Catalysis,
Debye Institute, University of Utrecht, Sorbonnelaan 16, PO Box 80083, 2508 TB Utrecht, The Netherlands,
and Centrum voor Oppervlaktechemie en Katalyse, Departement Interfasechemie, K.U. Leuven,
Kardinaal Mercierlaan 92, 3001 Heverlee, Belgium

Received: February 16, 2001; In Final Form: April 20, 2001

Silica-, alumina-, and zirconia-supported tantalum oxide and supported vanadia-tantala mixed oxide catalysts were investigated by XRD, UV−vis-DR, FTIR, and FT-Raman spectroscopy to determine the nature of the surface tantala species. Two types of surface TaO_x species were identified. On the SiO_2 support, at low coverages tetrahedral TaO_4 species exist, with a Ta═O bond and three bridging Ta−O-support bonds. At higher coverages, octahedral TaO_6 species occur. On Al_2O_3 and ZrO_2 both surface species exist already at considerably low Ta loading. The acidic properties of the catalysts were investigated by an FTIR study of adsorbed pyridine. Supported tantala is clearly more Lewis acidic in comparison to vanadia. The oxidation of methanol was used to probe the catalytic performance of the supported oxide species and from the activity and product distribution it is concluded that supported tantala predominantly shows acidic over redox behavior.

Introduction

Group V transition metal oxides are very efficient as catalysts in numerous processes. The physical, chemical and catalytic properties of supported vanadium and niobium oxides have been studied extensively in the past, using several spectroscopic characterization techniques and catalytic reactions. Vanadium oxide catalysts catalyze a number of industrially important processes. They have been used successfully in the selective oxidation of aliphatic and aromatic hydrocarbons (e.g., oxidation of methane to formaldehyde,[1] oxidation of *o*-xylene to phthalic anhydride[2−4]), the selective oxidation of SO_2 in the production of sulfuric acid,[5] and the selective catalytic reduction (SCR) of nitric oxide with ammonia[6,7]. In addition, the photocatalytic activity of vanadium oxide catalysts has been reported.[8] Niobium oxide catalysts exhibit poor performance as redox site during oxidation reactions.[9] Niobia possesses primarily (Lewis) acidic characteristics.[10] However, it remarkably enhances the catalytic activity and selectivity of several metal oxide catalysts, when used as additive or support (due to the higher acidity features).[11,12]

Studies on the molecular structure of supported VO_x and NbO_x have revealed that the supported metal oxide phase forms a two-dimensional overlayer on oxide supports such as silica alumina, zirconia, or titania.[4] There is a general consensus that, at low surface coverages, the vanadia species are present in an isolated tetrahedral VO_4 coordination, possessing a terminal V═O and three bridging V−O-support bonds. At higher surface vanadia coverages, the vanadia species are polymerized through bridging V−O−V bonds. With increasing surface coverage square pyramidal and octahedrally coordinated (and even crystalline) vanadia species occur. Similarly, supported niobia exhibits NbO_4 species at low coverage and polymerized NbO_6 species at high coverage.[9,13]

Tantalum oxide is used as optical coating or in electronics technology as capacitor material (because of its high dielectric constant).[14−16] However, the current knowledge of the physical and chemical properties of tantala is rather limited. Hydrated tantalum oxide ($Ta_2O_5{\cdot}nH_2O$) is highly acidic.[17] Ushikubo et al.[18,19] showed that silica-supported tantalum oxide catalyzes the vapor phase Beckmann rearrangement of cyclohexanone oxime to ε-caprolactam. Furthermore, it is reported that $SiO_2-Ta_2O_5$ mixed oxides exhibit unique properties in alcohol dehydration.[18,20]

In this paper, we report on the structural, chemical, and catalytic properties of SiO_2-, Al_2O_3-, and ZrO_2-supported tantalum oxide catalysts, using the supported vanadium oxide case for comparison. The supported tantala and vanadia catalysts were prepared by liquid- and gas-phase modification reactions starting from tantalum ethoxide ($Ta(OC_2H_5)_5$) and vanadyl acetylacetonate ($VO(acac)_2$), respectively. The reaction of the $VO(acac)_2$ complex with various supports has been described in detail in earlier publications.[21−27] It was demonstrated that the use of transition metal complexes in the preparation of uniform and disperse supported transition metal oxides is very successful. Similarly, Ushikubo et al.[19] showed that the dispersion and the catalytic performance of the supported tantalum oxide phase is much better when the synthesis is carried out using a tantalum alkoxide rather than by using aqueous impregnation.

---

* To whom correspondence should be addressed. E-mail: baltes@uia.ua.ac.be.

† Laboratory of Adsorption and Catalysis.

‡ Fortum Oil and Gas Oy.

§ Department of Inorganic Chemistry and Catalysis.

‖ Centrum voor Oppervlaktechemie en Katalyse.

10.1021/jp010628b CCC: $20.00

To investigate the TaO_x structure and surface properties, supported vanadia-tantala mixed oxides are prepared as well. The effect of Ta addition on the nature and surface properties of supported vanadia catalysts is discussed. Chemisorption of pyridine followed by IR characterization was applied to study the acidic properties of the catalysts. The oxidation of methanol was performed in order to investigate the redox behavior.

Experimental Section

The silica (Grace 432), γ-alumina (AKZO), and zirconia (MEL Chemicals) supports have a specific surface area (S_{BET}) of 300, 200, and 59 m^2/g, respectively, after pretreatment in air at 500 °C for 16 h.

In the liquid phase reactions, the thermally treated support was stirred at room temperature for 1 h in a zeolite-dried toluene solution containing tantalum ethoxide ($Ta(OC_2H_5)_5$, Fluka) or vanadyl acetylacetonate ($VO(acac)_2$, Fluka) for modification with Ta or V, respectively. The reaction vessel was purged with a stream of dry nitrogen. After the reaction the modified support was filtered, washed with fresh solvent and dried under vacuum at room temperature. Subsequently, the samples were calcined in air at 500 °C for 16 h.

The gas-phase reactions are performed by the Atomic Layer Deposition technique (ALD).[28−30] The thermally pretreated supports (3 g) were additionally preheated at the reaction temperature for 3 h in a fixed-bed flow-type reactor, under a pressure of 5−10 kPa in a nitrogen flow. After this pretreatment, the reactant vapors were passed through the support bed, with nitrogen used as carrier gas. Vaporization of the reactants was carried out by sublimation of $VO(acac)_2$ at 160 °C and evaporation of $Ta(OC_2H_5)_5$ at 200 °C, respectively. $VO(acac)_2$ was deposited at a reaction temperature of 160 °C, $Ta(OC_2H_5)_5$ at 200 °C. After the reaction, the modified support was purged with nitrogen at the reaction temperature for 2 h. Subsequently, calcination was performed in the reactor at 500 °C, in an airflow for 6h.

The liquid- and gas-phase preparations of the supported vanadia-tantala mixed oxides were carried out similarly, by successive modification of the support (followed by calcination before the next modification).

The Ta and V concentrations were determined by electron microprobe analysis and neutron activation analysis. In the liquid-phase modification, samples were prepared with varying metal loading (up to 0.8 mmol/g Ta and up to 1.0 mmol/g V), by using appropriate amounts of the transition metal precursors in the reaction solution. In the gas-phase modification, one reaction cycle was performed (i.e., deposition of the precursor until saturation of the support and subsequent calcination), which leads to V and Ta coverages listed in Table 1. The actual deposition process is discussed in detail in earlier publications.[21−25,28−30]

Pyridine adsorption was performed after calcination of the samples at 500 °C for 16h, and subsequent degassing at 150 °C for 3 h. The samples were exposed to pyridine vapor for 30 min. After evacuation for 3 h at 150 °C, the FTIR−PAS spectra were recorded.

Photoacoustic infrared spectra (FTIR−PAS) were measured on a Nicolet 20 SX spectrometer, equipped with a McClelland Photoacoustic cell. X-ray diffraction patterns were collected on a Philips PW1840 powder diffractometer (45 kV, 30 mA), using Ni-filtered CuKα radiation. UV−vis diffuse reflectance spectra (UV−vis-DRS) were obtained on a UNICAM 8700 UV−vis spectrometer, with a diffuse reflectance accessory using $BaSO_4$ standard white as reference. FT-Raman spectra were recorded on a Nicolet Nexus FT-Raman spectrometer with a Ge detector. All samples were measured at room temperature in a 180 degree reflective sampling configuration, with a 1064 nm Nd:YAG excitation laser.

TABLE 1: Ta and V Loading of the Liquid Phase and Gas Phase Prepared Supported Oxide Catalysts

	liquid-phase modification		gas-phase modification	
catalyst	V loading (mmol/g)	Ta loading (mmol/g)	V loading (mmol/g)	Ta loading (mmol/g)
VO_x/SiO_2	up to 1.00		0.49	
VO_x/Al_2O_3	up to 2.00		0.91	
VO_x/ZrO_2	up to 1.00		0.31	
TaO_x/SiO_2		up to 0.80		0.48
TaO_x/Al_2O_3		up to 0.80		0.55
TaO_x/ZrO_2		up to 0.60		0.16
VO_x-TaO_x/SiO_2	up to 1.00	up to 0.80	0.51	0.54
VO_x-TaO_x/Al_2O_3	up to 2.00	up to 0.80	0.87	0.34
VO_x-TaO_x/ZrO_2	up to 1.00	up to 0.60	0.29	0.15

The oxidation of methanol was carried out at 250 °C in a fixed-bed continuous flow reactor at atmospheric pressure. The amount of catalyst was controlled to obtain less than 10% methanol conversion. Prior to the reaction the catalyst was treated by flowing a He/O_2 mixture at 400 °C for 16 h, to remove physisorbed water. A 100 mL/min $He/O_2/MeOH$ (88/8/4 mol %) flow was used as reactant mixture. Reaction products were analyzed by gas chromatography on a 2 m × $^1/_8$ in. Porapak T column (Alltech Inc.).

Results

(1) Structural Characterization. *(A) XRD.* X-ray diffraction analysis was performed on the support materials and on the supported oxide catalysts. The silica and alumina supports are amorphous, whereas the zirconia support shows various reflections typical for the monoclinic crystal structure. The catalysts demonstrate a featureless XRD pattern, except for the characteristic pattern of the respective support materials, which suggests that the deposited oxide layers are amorphous.

(B) UV−Vis Diffuse Reflectance Spectroscopy. UV−vis-DRS is used to investigate the coordination of the supported oxide species, since the energy of the oxygen-to-metal charge transfer (CT) bands is dependent on the transition metal ion and on the number of oxygen atoms surrounding it. Therefore, UV−vis-DRS allows to distinguish between different types of transition metal oxide configurations present on the support. Supported vanadium oxides generally show several CT bands as a function of the vanadium loading, according to the presence of three main types of configurations:[25,31,32] tetrahedrally coordinated monomers and polymeric chains (characterized by CT bands between 200 and 400 nm), two-dimensional ribbons with a square pyramid coordination geometry (CT band at 410 nm) and octahedrally coordinated species (CT band at 470 nm). Figure 1 shows the UV−vis-DRS spectra of the tantalum oxide containing catalysts, prepared by liquid phase and gas phase. Pure Ta_2O_5 (where the central Ta^{5+} ion is in a octahedral configuration) shows a main absorption band at ∼270 nm.

(i) SiO_2. Silica-supported tantala (Figure 1A) exhibits at low loading (<0.5 mmol/g Ta) a strong band with maximum at 233 nm (Figure 1A, spectrum a). With higher loadings an additional band is present at 265 nm, and some absorption appears in the 300−350 nm region (spectrum b). Remarkably, the samples prepared by the ALD technique show better uniformity compared to the liquid-phase samples. The TaO_x/SiO_2 sample in

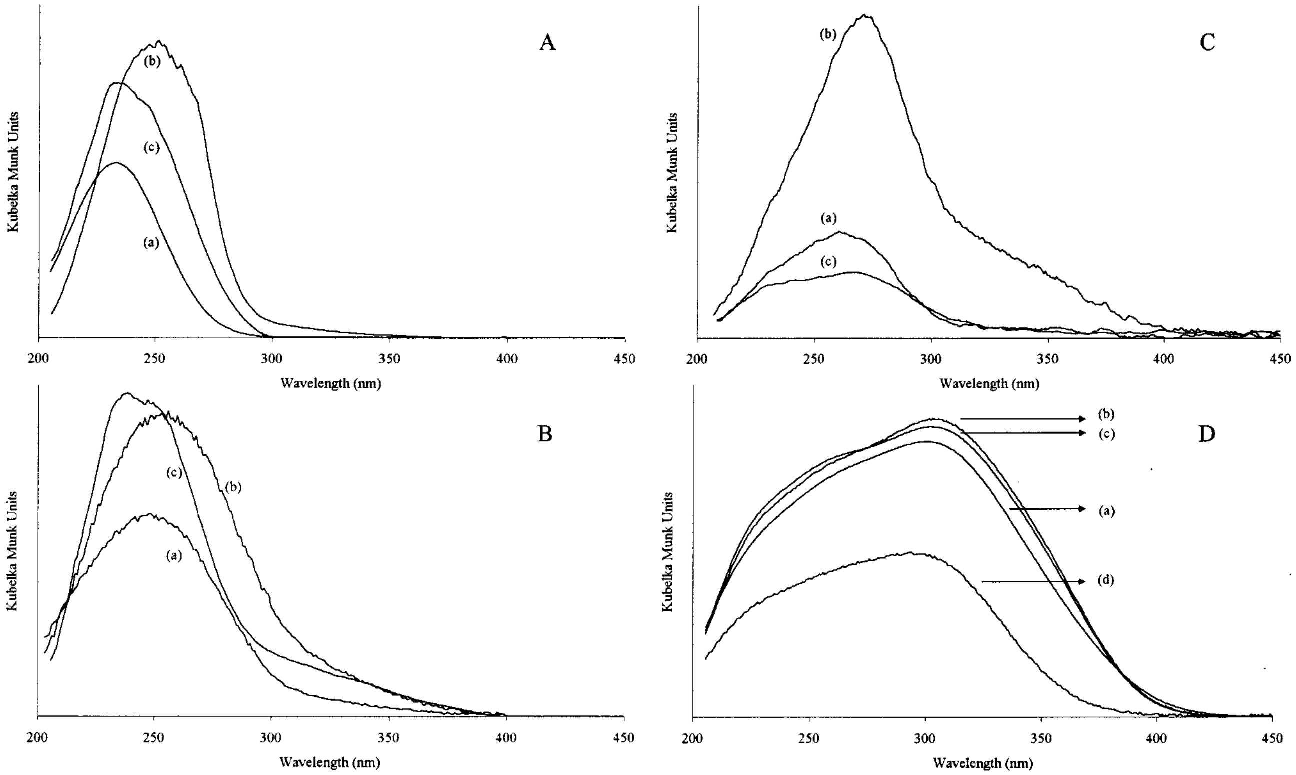

Figure 1. UV−vis diffuse reflectance spectra of the supported oxide catalysts. (A) TaO_x/SiO_2 catalysts; (a) liquid-phase sample 0.21 mmol/g; (b) liquid-phase sample 0.47 mmol/g; (c) ALD sample 0.48 mmol/g. (B) TaO_x/Al_2O_3 catalysts; (a) liquid-phase sample 0.20 mmol/g; (b) liquid-phase sample 0.80 mmol/g; (c) ALD sample 0.55 mmol/g. (C) TaO_x/ZrO_2 catalysts measured with zirconia as reference; (a) liquid-phase sample 0.15 mmol/g; (b) liquid-phase sample 0.60 mmol/g; (c) ALD sample 0.16 mmol/g. (D) Liquid phase prepared VO_x-TaO_x/SiO_2 catalysts with respective loadings of (a) 0.36 mmol/g V and 0 mmol/g Ta; (b) 0.36 mmol/g V and 0.20 mmol/g Ta; (c) 0.35 mmol/g V and 0.59 mmol/g Ta; (d) 0.20 mmol/g V and 0.60 mmol/g Ta.

Figure 1A, spectrum c, shows almost exclusive absorption at 233 nm, whereas the liquid-phase sample with the same loading already exhibits absorption at higher wavelengths.

(ii) Al_2O_3. Alumina-supported tantala (Figure 1B) also shows the CT band around 230 nm, but it already exhibits an absorption at higher wavelengths (265 nm) at considerably low loadings, even in the case of the ALD-prepared samples.

(iii) ZrO_2. The pure zirconia support is not transparent in the UV region studied. Therefore it is difficult to infer unambiguous information. However, when the UV−vis-DRS spectra are obtained with the zirconia support as reference (Figure 1C), similar bands with maxima around 235 and 270 nm are observed.

(iv) VO_x-TaO_x. The spectra of the supported vanadium−tantalum mixed oxides (in Figure 1D, the silica-supported catalysts are presented) show the same evolution as the spectra obtained for supported vanadium oxides. Increasing the vanadium concentration (with constant Ta concentration) results in typical charge-transfer transitions at higher wavelength, which shows that more polymerized VO_x species occur. However, increasing the Ta concentration (Figure 1D, spectra a−c) does not result in an appreciable change of the UV−vis-DRS spectra. In addition, there is no change when the sequence of grafting of vanadium oxide and tantalum oxide is reversed.

Figure 2 presents the UV−vis-DRS spectra of supported vanadia and tantala after hydration of the catalysts. Hydration (or exposure to ambient conditions) dramatically changes the molecular structure of the surface species, due to coordination of water molecules. In the case of supported vanadium oxide, these changes are easily observable, as the dehydrated white samples turn yellow or orange upon exposure to ambient air. Therefore, the UV−vis-DRS spectra of the hydrated vanadium oxide samples show significant absorption in the 400−600 nm region (Figure 2A). Hydration of the white supported tantala samples does not result in a change of color. Still, the hydrated tantala samples in Figure 2B show an increased absorption of the CT band around 260 nm and in the 300−350 nm region, suggesting a similar change of the TaO_x structures, due to the coordination of water.

(C) FTIR Spectroscopy. (i) OH Stretching Region. Infrared spectroscopy yields information on the interaction of the surface metal oxide species with the support, by examining the surface hydroxyl region. After the modification with TaO_x and/or VO_x, the IR intensity of the various OH bands of the SiO_2, Al_2O_3, and ZrO_2 supports decreases gradually with increasing loading, due to the consumption of the surface hydroxyls in the reaction with the respective transition metal precursors. Accordingly, the deposited oxide is linked to the support by support-oxygen−metal bonds. However, even at considerably high coverages, not all the surface OH groups are removed. On SiO_2, with increasing V and Ta coverage new bands appear at 3660 or 3680 cm^{-1} (spectra not shown), revealing the presence of V−OH[25] and Ta−OH[17] species, respectively. In the case of the alumina and zirconia-supported vanadia and tantala samples the interpretation of the appearance of these metal−OH species is difficult because of the IR bands of the support hydroxyls. However, at higher Ta loadings an increased intensity is observed of a band located at 3743 cm^{-1}, attributed to new OH groups generated on these samples.

(ii) Metal−Oxygen Region. The infrared spectra also show important vanadium−oxygen and tantalum−oxygen IR vibrations. Unfortunately, some of the metal−oxygen vibrations are obscured by the overlapping IR bands of the various supports.

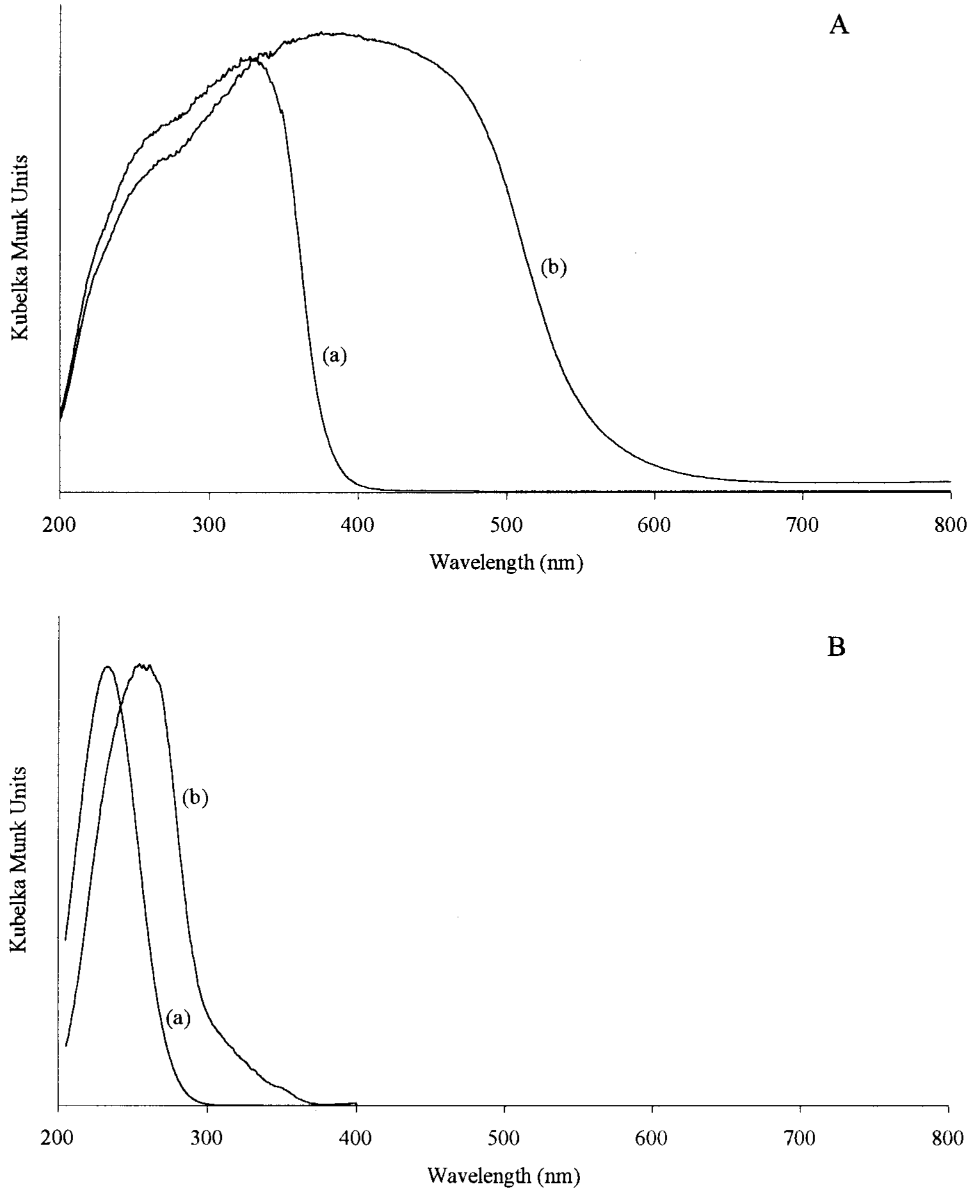

Figure 2. Influence of hydration on the structure of the supported oxide catalysts. UV−vis diffuse reflectance spectra of VO_x/SiO_2 (A) and TaO_x/SiO_2 (B) in the dehydrated (a) and hydrated (b) state.

In Figure 3, the IR spectra of the metal−oxygen region of the catalysts under study are shown. To clarify the occurring metal−oxygen species in the case of the alumina and zirconia-supported samples, difference spectra are presented after spectrum subtraction of the blank supports.

(a) SiO_2. In the case of the silica-supported vanadium oxide catalysts (Figure 3A, spectrum b), a band around 926 cm^{-1} is attributed to the presence of Si−O−V bonds.[25] Both liquid- and gas-phase-prepared TaO_x/SiO_2 samples show broad bands centered around 702 and 918 cm^{-1} (Figure 3A, spectrum c). The former corresponds to Ta−O stretching vibration modes.[33] The latter can be attributed to the presence of Si−O−Ta linkages in accordance to the vanadia case. Additionally, a clearly resolved band is observed at 976 cm^{-1}.

(b) Al_2O_3. The VO_x/Al_2O_3 samples (Figure 3B, spectrum a) show an IR absorption at 1025 cm^{-1}, assigned to the symmetric stretching vibration of terminal V═O[32,34] with three bridging V−O−Al linkages to the support surface. TaO_x/Al_2O_3 exhibits a band at 980 cm^{-1}. Remarkably, at higher Ta coverages (spectrum c) an absorption is observed at 2336 cm^{-1}. This is assigned to a stretching vibration mode of Ta═O bonds in an amorphous tantalum oxide overlayer.[35] It is located at 2335 cm^{-1} when an amorphous tantala phase is formed, and is shifted to 2340 cm^{-1} in crystalline tantala. The OH band at 3743 cm^{-1} which is generated simultaneously with the formation of this amorphous tantala layer, can therefore be attributed to Ta−OH species on the amorphous overlayer.

(c) ZrO_2. Zirconia-supported vanadia samples (Figure 3C, spectrum a) show an IR absorption at 1024 cm^{-1}, which can also be assigned to terminal V═O.[36] However, a band around 850−820 cm^{-1} is observed, which indicates the presence of V−O−V linkages. In contrast to silica and alumina, the zirconia-supported tantala (Figure 3, spectrum b) only shows a minor band at 980 cm^{-1} and a broad contribution of Ta−O vibrations is observed around 820 cm^{-1}. At higher Ta coverages, the presence of the 2336 cm^{-1} band reveals the formation of an amorphous tantala phase, similar to the alumina case.

(d) VO_x-TaO_x. The supported vanadia-tantala mixed oxide samples exhibit several bands of both the vanadia and tantala, showing the same evolution as a function of the loading as in the case of the supported oxides as such. When vanadia is deposited on the alumina- and zirconia-supported tantala

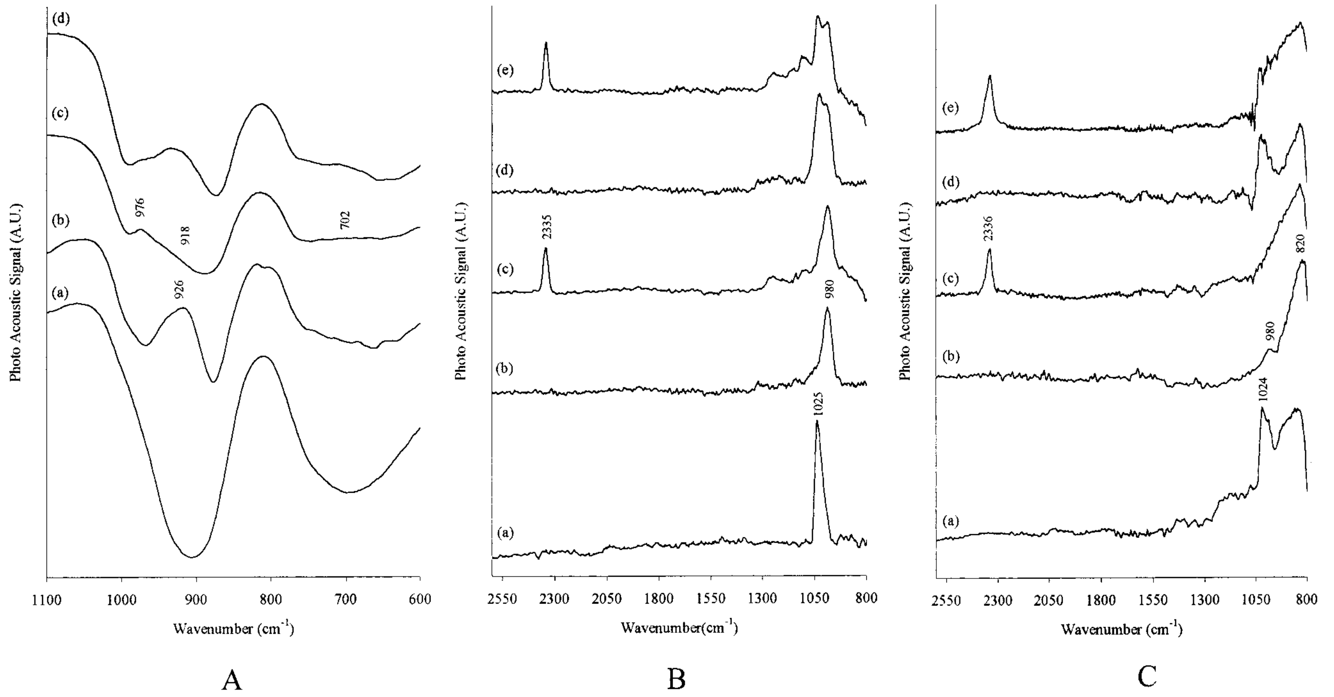

Figure 3. FTIR−PAS spectra of the liquid phase prepared supported oxide catalysts studied in the metal oxygen region. (A) Silica-supported oxide catalysts (a) pure SiO2 support after pretreatment at 500 °C; (b) VO_x/SiO_2 (0.36 mmol/g); (c) TaO_x/SiO_2 (0.47 mmol/g); (d) VO_x-TaO_x/SiO_2 with respective V and Ta loading of 0.35 and 0.20 mmol/g. (B) difference spectra of the alumina-supported oxide catalysts; after spectrum subtraction of blank alumina. (a) VO_x/Al_2O_3 (0.70 mmol/g); (b) TaO_x/Al_2O_3 (0.20 mmol/g); (c) TaO_x/Al_2O_3 (0.80 mmol/g); (d) VO_x-TaO_x/Al_2O_3 with respective V and Ta loading of 0.72 and 0.45 mmol/g; (e) VO_x-TaO_x/Al_2O_3 with respective V and Ta loading of 0.69 and 0.78 mmol/g. C: difference spectra of the zirconia-supported oxide catalysts; after spectrum subtraction of blank zirconia. (a) VO_x/ZrO_2 (0.37 mmol/g); (b) TaO_x/ZrO_2 (0.24 mmol/g); (c) TaO_x/ZrO_2 (0.60 mmol/g); (d) VO_x-TaO_x/ZrO_2 with respective V and Ta loading of 0.37 and 0.34 mmol/g; (e) VO_x-TaO_x/ZrO_2 with respective V and Ta loading of 0.37 and 0.57 mmol/g.

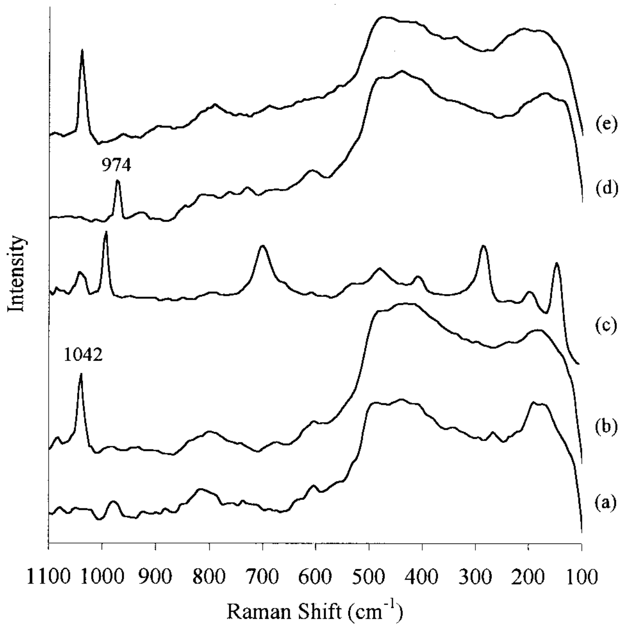

Figure 4. FT-Raman spectra of the silica-supported oxide catalysts; (a) pure SiO_2; (b) VO_x/SiO_2 (0.36 mmol/g); (c) VO_x/SiO_2 (1.03 mmol/g); (d) TaO_x/SiO_2 (0.47 mmol/g); (e) VO_x-TaO_x/SiO_2 with respective V and Ta loading of 0.35 and 0.59 mmol/g.

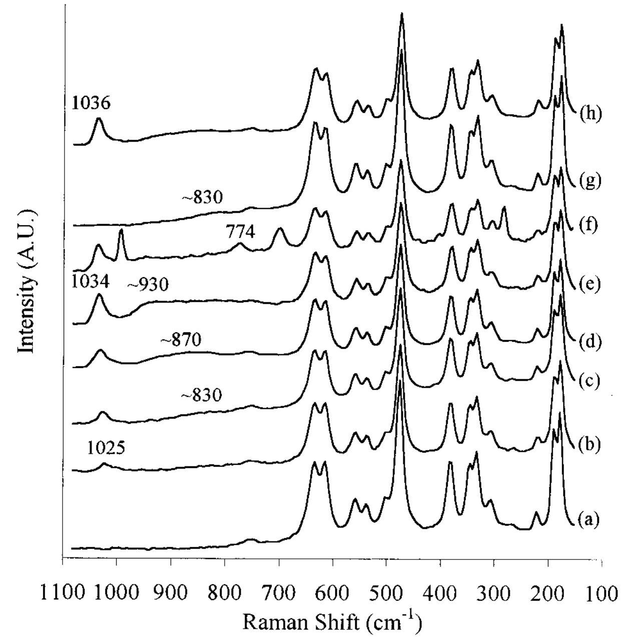

Figure 5. FT-Raman spectra of the zirconia-supported oxide catalysts; (a) pure ZrO_2; (b−f) VO_x/ZrO_2 with respective V loading of 0.09, 0.19, 0.37, 0.62, and 1.02 mmol/g; (g) TaO_x/ZrO_2 (0.24 mmol/g); (h) VO_x-TaO_x/ZrO_2 with respective V and Ta loading of 0.37 and 0.34 mmol/g.

samples, which already exhibit the amorphous tantalum oxide phase, it is observed that the intensity of the 3743 cm^{-1} band (Ta−OH) decreases. This suggests that a part of the vanadia species is linked to the tantala species.

(D) Raman Spectroscopy. Figures 4 and 5 show the FT-Raman spectra of the modified silica and zirconia samples. Unfortunately, the interpretation of the alumina-supported samples is complicated by a broad fluorescence background which overshadows the Raman features of the surface oxide species.

(i) SiO_2. Pure silica exhibits Raman modes at 430, 488, 605, 800, and 980 cm^{-1} (Figure 4a). Silica-supported vanadia in Figure 4b exhibits a strong Raman band at 1042 cm^{-1}, assigned to the stretching mode of V=O in a tetrahedral species with

three V−O−Si bonds to the silica surface.[25,32] At V loadings of >0.6 mmol/g, strong Raman features at 994, 697, 286, and 147 cm^{-1} (Figure 4c) reveal the formation of crystalline V_2O_5 (the XRD patterns could not evidence the presence of V_2O_5, which means that Raman spectroscopy is much more sensitive to small crystalline clusters). Silica-supported tantala (Figure 4d) shows a band at 974 cm^{-1}. The infrared study also showed a distinct band around 976 cm^{-1}. These bands are probably arising from Ta═O vibrations. Samples with Ta loadings of up to 0.8 mmol/g still show no bands of crystalline Ta_2O_5 (Raman bands[26,37] at 105, 253, and 627 cm^{-1}).

(ii) ZrO_2. The spectrum of the monoclinic zirconia sample has several strong bands at 634, 616, 476, 382, 334, 190, and 179 cm^{-1} (Figure 5a). Due to the influence of the oxide support the surface vanadium oxide band positions are shifted in comparison to the spectra of the silica-supported vanadia samples. On zirconia, the characteristic V═O band is observed at 1025 cm^{-1} (Figure 5b). Upon higher loadings, this band is gradually shifted to 1034 cm^{-1} (Figures 5c−e). In addition, broad bands appear around 830 cm^{-1} for low V loadings (Figure 5c), and at ∼870 and ∼930 cm^{-1} for higher V loadings (Figure 5, panels d and e). At low loadings, the Raman features indicate dispersed vanadia species. The bands at 1025 and 820 cm^{-1} are assigned to orthovanadate-like species in a tetrahedral coordination. The shift of the V═O band to higher values and the appearance of the 870 cm^{-1} band are due to the presence of dimeric or pyrovanadate-like (V_2O_7) species. At even higher coverages, the broad band around 930 cm^{-1} indicates the formation of polymerized surface vanadium oxide species, linked to each other by V−O−V bridges. At a V loading of 1 mmol/g (Figure 5f), bands at 994, 701, and 408 reveal the formation of V_2O_5 and a band at 774 shows the presence of a small ZrV_2O_7 phase, which is due to zirconia migration into the V_2O_5 crystallites.[38] Remarkably, samples up to a loading of 0.7 mmol/g (spectrum 5e) exhibit no bands indicative of the formation of ZrV_2O_7. Many other investigations already observe a quite strong ZrV_2O_7 band at intermediate loadings.[27,39] It demonstrates that the preparation method starting form $VO(acac)_2$ is beneficial in the creation of highly dispersed supported vanadium oxides.

The zirconia-supported tantala (Figure 5g) shows a broad Raman feature around 830 cm^{-1}. The intensity of this band increases with higher loadings. It is attributed to the surface oxide species linked to eachother by Ta−O−Ta species. The infrared study of the supported tantala samples at quite high coverages showed the presence of an amorphous Ta_2O_5 phase (IR band at 2335 cm^{-1}). The presence of microcrystalline tantalum oxide clusters, however, cannot be inferred from the Raman spectra due to the strong bands of the zirconia support.

(iii) VO_x-TaO_x. The spectra of the supported vanadia-tantala mixed oxide catalysts (Figure 4e and Figure 5h) are similar to the supported vanadia samples. Suprisingly, they show no Raman features arising from the tantala phase. This is probably due to the low cross-section of the tantalum−oxygen vibrations compared to the vanadium−oxygen vibrations, as reported for the niobia-vanadia system.[11] No changes in the Raman spectra are observed upon addition of tantalum oxide to the silica-supported vanadia samples, nor when the vanadia phase is deposited on a previously prepared silica-supported tantala phase (the V═O band is observed at 1042 cm^{-1}). In the case of the zirconia samples (Figure 5h), the V═O band is somewhat shifted to higher values upon addition of tantala, but there is no gradual change with increasing Ta loading. In addition, the vanadia-tantala samples exhibit no bands attributed to polymeric V−O−V species (at 930 cm^{-1}), which means that the vanadia phase rests well-dispersed over the support surface and is not forced to aggregate upon Ta addition.

(2) Surface Properties. *(A) Acidic Properties: Adsorption of Pyridine.* The spectroscopic study of adsorbed pyridine is a useful method to determine the catalysts' surface acidity, as it enables to distinguish between Brønsted and Lewis acid sites. The type of interaction between the adsorbed pyridine and the acid sites on the catalyst surface gives rise to several characteristic infrared bands.

Typical IR absorption bands of pyridine adsorbed on Brønsted acid sites (BPy) are found around 1491, 1545, 1578, and 1640 cm^{-1}, whereas Lewis acidity gives rise to pyridine bands (LPy) around 1450, 1491, 1578, and 1612 cm^{-1}.[10,40−42] The ratio of the areas under the bands around 1545 cm^{-1} (BPy) and 1450 cm^{-1} (LPy) is usually related to the ratio of concentrations of Brønsted to Lewis acidity (B/L).[41] The exact positions of the 1450 and 1612 cm^{-1} LPy bands are sensitive to the strength of the Lewis acidity.

Figure 6 presents the infrared spectra of the supports and supported metal oxides under study, after adsorption of pyridine and degassing at 150 °C (in order to avoid the presence of physisorbed pyridine). SiO_2 exposed to pyridine vapor (Figure 6A, spectrum a) shows no characteristic bands of the adsorbed base, indicating that the silica surface exhibits no Brønsted nor Lewis acidity. In contrast, alumina contains strong Lewis acid sites, giving rise to LPy bands at 1449, 1491 and 1614 cm^{-1} (Figure 6B, spectrum a). The infrared spectrum of the zirconia support after adsorption of pyridine (Figure 6C, spectrum a), shows bands at 1445, 1488, and 1608 cm^{-1}, attributed to Lewis acidity. In addition, a small contribution at 1542 cm^{-1} indicates the presence of Brønsted sites (surface OH groups). From the position of the LPy bands it is inferred that the Lewis sites on zirconia are clearly weaker than the Lewis sites on alumina.

The supported vanadium oxide shows bands typical of both Lewis and Brønsted acidity. Supported tantalum oxide catalysts exhibits only LPy bands at low coverages. At higher Ta loadings Brønsted acidity occurs as well (in accordance with the formation of Ta−OH species at higher loadings, see infrared discussion above). Still, from the Brønsted-to-Lewis ratio (B/L) obtained after integration of the bands around 1545 cm^{-1} (BPy) and 1450 cm^{-1} (Lpy) (presented in Table 2), it can be inferred that the supported tantala samples exhibit more Lewis acidity in comparison to supported vanadia. In addition, the supported vanadia-tantala mixed oxides show an increased Lewis acidity (B/L decreases), with increasing Ta content. Clearly, supported tantalum oxide exhibits predominantly Lewis acidic characteristics. Furthermore, the position of the LPy bands indicate, that the Lewis acid sites on the surface of the silica and alumina-supported tantala catalysts are stronger than the Lewis acid sites on TaO_x/ZrO_2.

(B) Catalytic Performance in the Oxidation of Methanol. The oxidation of methanol is a useful test reaction to study the redox behavior of the supported oxide catalysts. It is commonly used as a catalytic surface probe, as it leads to various products according to the chemical composition or arrangement of the surface atoms.[4,43,44] The product selectivity reflects the presence of acidic, basic, or redox sites. Acidic sites give rise to dimethyl ether, basic sites produce carbon oxides (CO_x) and redox sites produce formaldehyde, methyl formate, and dimethoxymethane. In Tables 2, 3, and 4 the results are presented of the oxidation of methanol for the catalysts under study.

(i) SiO_2. Pure silica shows very poor catalytic performance. The activity of the silica-supported vanadium oxide is signifi-

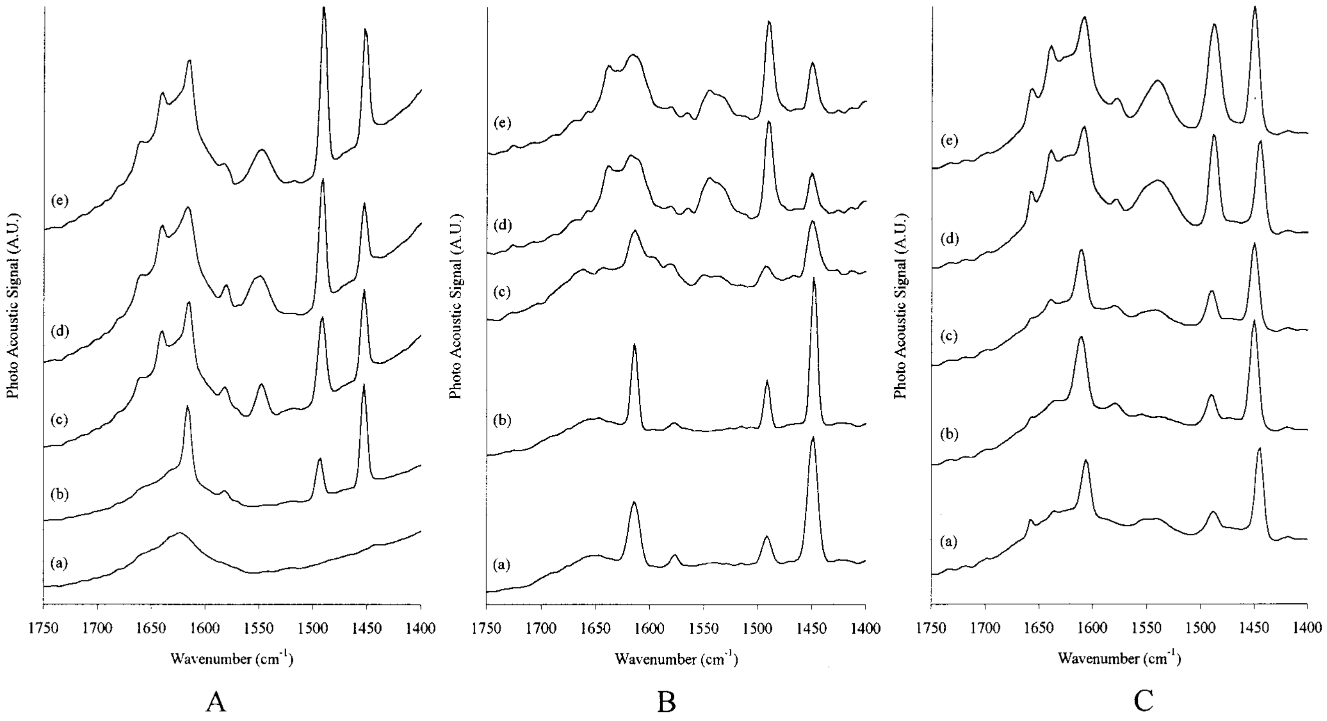

Figure 6. FTIR spectra of pyridine adsorbed on (A) silica-supported oxide catalysts; (a) pure SiO_2; (b) TaO_x/SiO_2 (0.21 mmol/g); (c) TaO_x/SiO_2 (0.47 mmol/g); (d) VO_x/SiO_2 (0.37 mmol/g); (e) VO_x-TaO_x/SiO_2 with respective V and Ta loading of 0.37 and 0.20 mmol/g, and (B) alumina-supported oxide catalysts; (a) pure Al_2O_3; (b) TaO_x/Al_2O_3 (0.20 mmol/g); (c) TaO_x/Al_2O_3 (0.80 mmol/g); (d) VO_x/Al_2O_3 (0.70 mmol/g); (e) VO_x-TaO_x/Al_2O_3 with respective V and Ta loading of 0.72 and 0.45 mmol/g. C: Zirconia-supported oxide catalysts; (a) pure ZrO_2; (b) TaO_x/ZrO_2 (0.24 mmol/g); (c) TaO_x/ZrO_2 (0.60 mmol/g); (d) VO_x/ZrO_2 (0.37 mmol/g); (e) VO_x-TaO_x/ZrO_2 with respective V and Ta loading of 0.37 and 0.34 mmol/g.

TABLE 2: Activity and Selectivity of the SiO_2 Supported VO_x, TaO_x and VO_x-TaO_x Catalysts

							selectivity (%)[e]			
catalyst	V (mmol/g)	Ta (mmol/g)	A[a] (10^{-3} mol/g h)	TOF[b] (10^{-3} s^{-1})	TOF_{redox}[c] (10^{-3} s^{-1})	TOF_{acid}[d] (10^{-3} s^{-1})	CO_x	FA	DME	MF
SiO_2	0.00	0.00	1.00				0.0	2.3	86.1	11.6
VO_x/SiO_2	0.20	0.00	4.99	6.92	6.72	0.20	0.0	25.1	2.9	72.0
VO_x/SiO_2	0.36	0.00	5.23	4.04	3.83	0.21	0.0	45.2	5.1	49.7
VO_x/SiO_2	0.70	0.00	5.98	2.37	1.80	0.53	1.9	47.1	22.3	28.7
VO_x/SiO_2	1.03	0.00	5.23	1.41	0.89	0.35	12.3	45.8	24.6	17.3
TaO_x/SiO_2	0.00	0.24	3.99	4.62	0.00	4.62	0.0	0.0	100.0	0.0
TaO_x/SiO_2	0.00	0.47	5.28	3.12	0.94	2.19	0.0	14.0	70.0	16.0
VO_x-TaO_x/SiO_2[f]	0.36	0.20	5.48				0.0	74.8	25.2	0.0
VO_x-TaO_x/SiO_2[f]	0.35	0.59	6.03				0.0	54.8	40.3	4.9
VO_x-TaO_x/SiO_2[f]	0.24	0.60	5.08				0.0	47.5	26.6	25.9
TaO_x-VO_x/SiO_2[g]	0.37	0.20	5.98				0.0	74.3	25.0	0.7

[a] Activity, moles of methanol converted per gram of catalyst and per hour. [b] Turnover frequency, moles of methanol converted per mole of metal and per second. [c] Turnover frequency based on the amount of redox products (FA + MF). [d] Turnover frequency based on the amount of DME. [e] FA, formaldehyde; DME, dimethyl ether; MF, methyl formate. [f] Sample prepared by deposition of TaO_x prior to deposition of VO_x. [g] Sample prepared by deposition of VO_x prior to deposition of TaO_x.

cantly higher. VO_x/SiO_2 produces mainly oxidation products (formaldehyde and methyl formate). The high selectivity for methyl formate substantiates the high dispersion of the vanadium oxide species on the silica support.[45] The catalyst surface exhibits an even distribution of vanadia and residual hydroxyl groups of the silica support. Methanol is adsorbed and transformed to formaldehyde on the vanadium sites. However, methanol can react with the residual surface hydroxyl sites as well, which results in adsorbed methoxy groups.[46,47] Therefore, during the methanol conversion, the formaldehyde formed on the vanadia sites is in close interaction with methoxy groups on the silica sites. Via a hemiacetal intermediate, methyl formate is produced.[45] With increasing loadings, the formaldehyde selectivity increases, as the surface density of the residual Si−OH groups decreases. For the silica samples with V loadings at which crystalline V_2O_5 is observed (>0.6 mmol/g), the formation of redox products markedly decreases, in favor of the formation of dimethyl ether and carbon oxides.

Silica-supported tantalum oxide catalysts show activities comparable to the VO_x/SiO_2. However, the main reaction product is dimethyl ether, indicating the acidic properties of the TaO_x phase. Remarkably, at higher Ta loading the TaO_x/SiO_2 samples produce methyl formate and formaldehyde along with the formation of dimethyl ether. This suggests that the interaction of tantala with the silica support gives rise to a considerable redox activity too.

(ii) Al_2O_3. Alumina is very active for the dehydration of methanol to dimethyl ether, due to the strong acidity of the alumina surface sites. Deposition of vanadium oxide leads to a decreasing activity and increasing formaldehyde selectivity as a function of the vanadium loading. Moreover, the main product of the reaction is still dimethyl ether, which suggests that the

TABLE 3: Activity and Selectivity of the Al_2O_3 Supported VO_x, TaO_x, and VO_x-TaO_x Catalysts

catalyst	V (mmol/g)	Ta (mmol/g)	A^a (mol/g·h)	TOF^b (s^{-1})	$TOF_{redox}{}^c$ (s^{-1})	$TOF_{acid}{}^d$ (s^{-1})	selectivity (%)^e CO_x	FA	DME	MF
Al_2O_3	0.00	0.00	0.96				0.0	0.0	100.0	0.0
VO_x/Al_2O_3	0.25	0.00	0.97	1.07	0.02	1.05	0.0	2.3	97.7	0.0
VO_x/Al_2O_3	0.70	0.00	0.85	0.34	0.05	0.29	0.0	14.0	86.0	0.0
VO_x/Al_2O_3	1.20	0.00	0.70	0.16	0.04	0.12	0.0	21.7	77.3	1.0
VO_x/Al_2O_3	2.10	0.00	0.50	0.07	0.02	0.04	2.0	29.1	67.9	1.0
TaO_x/Al_2O_3	0.00	0.20	0.78	1.08	0.00	1.08	0.0	0.0	100.0	0.0
TaO_x/Al_2O_3	0.00	0.80	0.53	0.18	0.00	0.18	0.0	0.0	100.0	0.0
VO_x-$TaO_x/Al_2O_3{}^f$	0.72	0.45	0.50				0.0	13.1	86.9	0.0
TaO_x-$VO_x/Al_2O_3{}^g$	0.69	0.41	0.50				0.0	12.8	87.2	0.0

[a] Activity, moles of methanol converted per gram catalyst and per hour. [b] Turnover frequency, moles of methanol converted per mole of metal and per second. [c] Turnover frequency based on the amount of redox products (FA + MF). [d] Turnover frequency based on the amount of DME. [e] FA, formaldehyde; DME, dimethyl ether; MF, methyl formate. [f] Sample prepared by deposition of TaO_x prior to deposition of VO_x. [g] Sample prepared by deposition of VO_x prior to deposition of TaO_x.

TABLE 4: Activity and Selectivity of the ZrO_2 Supported VO_x, TaO_x, and VO_x-TaO_x Catalysts

catalyst	V (mmol/g)	Ta (mmol/g)	A^a (mol/g·h)	TOF^b (s^{-1})	$TOF_{redox}{}^c$ (s^{-1})	$TOF_{acid}{}^d$ (s^{-1})	selectivity (%)^e CO_x	FA	DME	MF
ZrO_2	0.00	0.00	0.05				0.0	0.0	15.2	84.8
VO_x/ZrO_2	0.09	0.00	0.55	1.69	1.53	0.16	0.0	68.3	9.7	22.0
VO_x/ZrO_2	0.19	0.00	0.65	0.95	0.91	0.04	0.0	87.1	3.8	9.1
VO_x/ZrO_2	0.36	0.00	1.00	0.77	0.76	0.01	0.0	92.0	1.7	6.3
VO_x/ZrO_2	1.02	0.00	0.55	0.15	0.12	0.01	10.3	74.9	8.1	6.7
TaO_x/ZrO_2	0.00	0.15	0.03	0.06	0.05	0.02	0.0	0.0	28.4	71.6
TaO_x/ZrO_2	0.00	0.24	0.03	0.04	0.01	0.03	0.0	0.0	83.8	16.2
VO_x-$TaO_x/ZrO_2{}^f$	0.36	0.05	0.98				0.0	92.0	4.0	4.0
VO_x-$TaO_x/ZrO_2{}^f$	0.36	0.17	0.98				0.0	92.2	4.9	2.9
VO_x-$TaO_x/ZrO_2{}^f$	0.36	0.34	0.97				0.0	91.0	6.0	3.0
VO_x-$TaO_x/ZrO_2{}^f$	0.36	0.58	0.64				0.0	88.7	7.7	3.6
TaO_x-$VO_x/ZrO_2{}^g$	0.35	0.20	0.98				0.0	92.5	5.8	1.7

[a] Activity, moles of methanol converted per gram of catalyst and per hour. [b] Turnover frequency, moles of methanol converted per mole of metal and per second. [c] Turnover frequency based on the amount of redox products (FA + MF). [d] Turnover frequency based on the amount of DME. [e] FA, formaldehyde; DME, dimethyl ether; MF, methyl formate. [f] Sample prepared by deposition of TaO_x prior to deposition of VO_x. [g] Sample prepared by deposition of VO_x prior to deposition of TaO_x.

TABLE 5: Summary of the Spectral Features of the Supported Vanadia and Supported Tantala Catalysts

UV-VIS-DR charge transfer band assignments

nature of species	CT band position (nm) VO_x	TaO_x
tetrahedral monomer	250, 300	230
tetrahedral chains	350	
square pyramidal	410	
octahedral	470	265

FTIR band assignments

infrared vibration	IR band position (cm^{-1}) SiO_2	Al_2O_3	ZrO_2
V−OH	3660	3660	3660
V═O		1025	1024
V−O−support	930		
V−O−V			840
Ta−OH	3680	3743	3743
Ta═O	976	980, 2336	980, 2336
Ta−O−support	918		
Ta−O−Ta			840

Raman band assignments

Raman vibration	Raman shift (cm^{-1}) SiO_2	Al_2O_3	ZrO_2
V═O	1042	1026	1025−1030
V−O−V			850−820
Ta═O	974	980	980
Ta−O−Ta			840−820

alumina acid sites are much more active than the redox activity of the vanadia sites.

Alumina-supported tantala shows exclusive dehydration activity. Increasing the Ta loading on alumina also results in decreasing activity, which indicates that the surface TaO_x sites (although acidic) are less active than the active sites of the alumina surface. Therefore, the overall activity of the TaO_x/Al_2O_3 samples is attributed to the reactivity of the support sites rather than on the reactivity of the tantala sites.

(iii) ZrO_2. Pure zirconia exhibits some redox activity and produces methyl formate, besides some dimethyl ether rising from the acidic surface sites. Deposition of vanadium oxide significantly increases the activity and leads to a quite selective formation of formaldehyde (except for samples containing crystalline fractions of V_2O_5).

Deposition of TaO_x on zirconia leads to a slightly increased activity in comparison to the pure support. The acidic properties of the tantala sites result in a marked increase of the dimethyl ether selectivity.

It is well established that supported vanadium oxide catalysts show quite different activity and selectivity when the support is changed. A readily reducible oxide support surface gives rise to a more active supported vanadium oxide phase.[4,48] This means that the reactivity depends on the reduction characteristics of the V−O-support bonds rather than the characteristics of the terminal V═O bonds. As a result, the redox activity of the supported vanadium oxides increases in the order $SiO_2 < Al_2O_3 < ZrO_2 \cong TiO_2$ according to the better surface reducibility of the support. This can also be inferred from the TOF_{redox} values of the VO_x/SiO_2, VO_x/Al_2O_3 and VO_x/ZrO_2 catalysts in Tables 2, 3, and 4. However, the correlation between activity of the surface tantala species and the surface reducibility of the support is not like in the case of vanadia. The total activity increases in the order $SiO_2 < Al_2O_3 < ZrO_2$, similar to the vanadia case. However, the main product of the reaction is dimethyl ether (except for some methyl formate on the ZrO_2 supported samples, which is due to the contribution of exposed zirconia redox sites), which shows that the tantalum oxide exhibits predominantly acidic characteristics. In addition, the total activity of the silica-supported tantala is almost the same as silica-supported vanadia, while the total activity of the zirconia-supported tantala is much lower than the vanadia analogue. Clearly, the reducibility of the support surface has a much stronger effect on the surface vanadia species than on the surface tantala sites.

(iv) VO_x-TaO_x. The difference in reactivity between vanadia and tantala is also reflected in the supported mixed oxide catalysts. The addition of tantala to silica-supported vanadia increases the total activity and the selectivities toward formaldehyde and dimethyl ether. On the other hand, the addition of tantala to alumina- and zirconia-supported vanadia does not affect the catalytic performance, which substantiates that on readily reducible supports the vanadia sites are much more active than the tantala sites. In addition, reversing the sequence of deposition of VO_x and TaO_x does not lead to significant changes in activity and selectivity. The only exception is the zirconia-supported catalyst prepared by the deposition of vanadium oxide on the amorphous tantalum overlayers (samples with high Ta loadings). The activity of this sample is significantly lower, although the selectivity pattern is the same as for the other zirconia-supported mixed vanadia-tantala. In this case a part of the vanadia sites is linked to the tantalum oxide overlayer. Apparently, the poor reducibility of the tantala phase leads to a decreased activity of these vanadia sites.

Discussion

Molecular Structures and Surface Properties of Tantalum Oxide Containing Catalysts. The supported tantalum oxide catalysts investigated clearly show the existence of two types of surface configurations, depending on the properties of the oxide support and the surface coverage. The spectral features of the supported oxide catalysts obtained in this study are summarized in Table 5.

TaO_x/SiO_2. The spectroscopic study of the silica-supported tantala catalyst shows at low Ta loading a highly uniform surface structure, characterized by a charge-transfer band in the UV−vis-DRS spectra at 233 nm, and Ta═O bands at 974 and 976 cm^{-1} in Raman and infrared, respectively. The Ta═O species are linked to the silica support by Si−O−Ta bridges, which is inferred from the consumption of Si−OH groups after deposition of the tantala phase, and the appearance of a broad IR band at 918 cm^{-1}. A recent EXAFS study of silica-supported tantalum oxide[49] revealed that the surface oxide species are present as isolated tantalate species with one short Ta−O bond and three long Ta−O bonds. This means that at low loadings the deposited TaO_x species are in an isolated tetrahedral configuration. However, the spectroscopic results from this study suggest that at higher loadings an additional surface configuration occurs, which gives rise to a CT band around 260 nm and exhibits Ta−OH species (IR band at 3680 cm^{-1}). On the other hand, the octahedrally coordinated Ta in pure Ta_2O_5 shows similar spectroscopic features. Therefore, the second surface structure is attributed to octahedrally coordinated tantala, which is probably polymerized via Ta−O−Ta bridges.

Furthermore, it seems that higher Ta loadings can be achieved by the ALD gas phase technique in comparison to the liquid phase synthesis, before octahedral (and probably polymerized) tantala species occur. The difference between gas and liquid phase can be explained by the structure of the tantalum ethoxide precursor. Most simple tantalum alkoxides adopt binuclear structures ($Ta_2(OR)_8(\mu\text{-}OR)_2$), with two bridging alkoxide ligands. Evaporation of the alkoxide occurs only after dissociation to monomers ($Ta(OR)_5$).[16] This means that during the ALD process monomeric species are interacting with the support surface, resulting in a much better distribution of isolated tantalum centers over the support surface. Still, liquid-phase samples with loadings up to 0.8 mmol/g (15 wt % Ta) show no evidence for the formation of crystalline Ta_2O_5.

The pyridine adsorption experiments showed that the silica-supported tantala phase is mainly Lewis acidic, although at high loadings also Brønsted acidity occurs, due to the presence of the Ta−OH groups. In the oxidation of methanol the supported tantala catalysts show excellent dehydration performance due to the acidic properties, but at higher loadings the interaction between tantala and silica causes some redox activity as well. This may be due to the ease of hydrolysis of the bridging Ta−O−Si bonds during the methanol oxidation, as reported for the silica-supported niobia case.[46,50] However, a detailed understanding for this redox behavior is not yet established and a thorough oxidation study is required in order to clarify this issue.

TaO_x/Al_2O_3. The alumina-supported tantalum oxides also exhibit CT band around 235 nm which indicates that the tantalum species are present in an isolated tetrahedral configuration. However, absorption at 265 nm suggests that even at low coverages a minor part of the TaO_x is octahedrally coordinated, even in the case of the ALD-prepared samples. Ta═O species are observed by an IR absorption at 980 cm^{-1}. At higher coverages an amorphous tantalum oxide overlayer exists, giving rise to an IR band at 2336 cm^{-1} and Ta−OH species at 3743 cm^{-1} (the band at 3680 cm^{-1} which is also associated with Ta−OH cannot be distinguished unambiguously due to the IR bands of the support hydroxyls).

The Ta sites supported on alumina show Lewis acidity and an exclusive dehydration activity in the oxidation of methanol. However, the alumina sites exhibit much higher activity than the tantala sites.

TaO_x/ZrO_2. On zirconia, the majority of the tantala species is in a polymeric octahedral coordination, even at low loadings, which is substantiated by the CT band at 270 nm and the Ta−O−Ta vibrations around 820−830 cm^{-1} in infrared and Raman. Similar to the alumina samples, the zirconia-supported tantala shows IR absorption at 2335 and 3743 cm^{-1} at higher coverages, indicating the presence of an amorphous Ta_2O_5 layer.

Zirconia-supported tantalum oxide is also Lewis acidic, which results in an almost exclusive dehydration activity in the oxidation of methanol.

It is concluded that at low Ta coverage the tantala species have exclusively T_d symmetry on silica, whereas both T_d and O_h symmetry of Ta is observed on alumina, and mainly O_h symmetry of Ta is observed on zirconia. This can be explained by the fact that metal ions in an overlayer at low coverage assume the symmetry of the support metal ions. It is known that silica shows only T_d symmetry,[51] whereas alumina shows a surface constructed of both T_d and O_h symmetries,[52,53] and zirconia shows only O_h symmetry[54] if one considers both nearest and next-nearest oxygen atoms.

Supported VO_x-TaO_x Mixed Oxides. The spectroscopic and catalytic comparison between supported vanadia and tantala oxide was very useful to deduce valuable information on the tantalum oxide structure and properties. The spectroscopic study of the supported mixed oxides leads to similar conclusions as in the case of the supported tantala and supported vanadia as such. Interestingly, the structure and dispersion of one metal oxide species is nearly unaffected by the presence of the other metal oxide species nor by the grafting sequence of the oxides.

The catalytic properties are significantly determined by the oxide support. Silica-supported vanadia-tantala catalysts exhibit high selectivity toward formaldehyde and dimethyl ether, according to the presence of both active redox and active acid centers. In contrast, on a readily reducible support like ZrO_2, the vanadia species are much more active than the tantala sites. In fact, the oxidation of methanol requires only one active surface site; therefore, the catalytic performance of the zirconia-supported catalysts is not promoted by the tantala species. Consequently, a mixed vanadia-tantala catalyst is useful for reactions that require both active redox and efficient acidic surface sites.

Conclusions

(1) Supported tantalum oxide show basically two types of molecular structures. On silica at low coverages, isolated tetrahedral species occur, with a short Ta═O bond and three bridging Ta−O-support bonds. At higher coverages, octahedrally coordinated tantala species occur. The alumina-supported tantala shows both surface species already at low coverages, whereas the zirconia samples predominantly exhibit polymerized, octahedrally configured tantalum oxide. In addition, the formation of an amorphous surface overlayer is revealed on both alumina and zirconia at high tantala coverages.

(2) The atomic layer deposition of the tantalum ethoxide precursor results in a better uniformity of the surface tantala species in comparison to the liquid phase. This is due to the binuclear structure of the tantalum alkoxide in the liquid phase, and the dissociation to a monomeric structure after evaporation.

(3) The supported tantala catalysts possess unique surface properties. The infrared study of the adsorption of pyridine showed the Lewis acidic characteristics of the surface tantala species. This is also reflected in the oxidation of methanol, which reveals that the supported tantala shows unique acidic properties. Suprisingly, the interaction of tantala with the silica support induces redox properties too.

(4) Supported vanadia-tantala mixed oxides are very well dispersed on the support surfaces. The grafting sequence does not lead to significant changes in surface structure or methanol oxidation performance. The ternary vanadia-tantala-support catalyst system is potentially useful in reactions requiring both redox and acid sites.

Acknowledgment. This work was supported by the FWO Vlaanderen (Research project G.0446.99). M. Baltes thanks the European Science Foundation (ESF) for a short-term fellowship in the scope of the ESF network on *"Elementary Steps of Layer Growth in the Fabrication of Novel Materials by Atomic Layer Epitaxy"*, for a research stay at Fortum Oil and Gas Oy, Espoo, Finland. P. Van Der Voort is a postdoctoral fellow of the F.W.O. Vlaanderen. The authors are grateful to Mrs. Minna Helsto and Mrs. Mirja Rissanen for their aid in the experimental work.

References and Notes

(1) Koranne, M.; Goodwin, J. G.; Marcelin, G. *J. Catal.* **1994**, *148*, 388.

(2) Dias, C. R.; Portela, M. F.; Bond, G. C. *J. Catal.* **1995**, *157*, 344.

(3) Bond, G. C.; Tahir, S. F. *Appl. Catal.* **1991**, *71*, 1.

(4) Deo, G.; Wachs, I. E.; Haber J. *Crit. Rev. Surf. Chem.* **1994**, *4*, 141.

(5) Dunn, J. P.; Stenger, H. P.; Wachs, I. E. *Catal. Today* **1999**, *51*, 301.

(6) Vogt, E. T. V.; Boot, A.; van Dillen, A. J.; Geus, J. W.; Janssen, F. J. J. G.; van den Kerkhof, F. M. G. *J. Catal.* **1988**, *114*, 313.

(7) Wachs, I. E.; Deo, G.; Weckhuysen, B. M.; Andreini, A.; Vuurman, M. A.; de Boer, M.; Amiridis, M. D. *J. Catal.* **1996**, *161*, 211.

(8) Tran, K.; Hanning-Lee, M. A.; Biswas, A.; Stiegman, A. E.; Scott, G. W. *J. Am. Chem. Soc.* **1995**, *117*, 2618.

(9) Wachs, I. E.; Briand, L. E.; Jehng, J. M.; Burcham, L.; Gao, X. *Catal. Today* **2000**, *57*, 323.

(10) Datka, J.; Turek, A. M.; Jehng, J. M.; Wachs, I. E. *J. Catal.* **1992**, *135*, 186.

(11) Deo, G.; Wachs, I. E. *J. Catal.* **1994**, *146*, 335.

(12) Viparelli, P.; Ciambelli, P.; Lisi, L.; Ruoppolo, G.; Russo, G.; Volta, J. C. *Appl. Catal., A* **1999**, *184*, 291.

(13) Jehng, J. M.; Wachs, I. E. *J. Phys. Chem.* **1991**, *95*, 7373.

(14) Kukli, K.; Ritala, M.; Matero, R.; Leskelä, M. *J. Cryst. Growth* **2000**, *212*, 459.

(15) Meng, J. F.; Rai, B. K.; Katiyar, R. S.; Bhalla, A. S. *J. Phys. Chem. Solids* **1997**, *58*, 1503.

(16) Pollard, K. D.; Puddephatt, R. J. *Chem. Mater.* **1999**, *11*, 1069.

(17) Ushikubo, T. *Catal. Today* **2000**, *57*, 331.

(18) Ushikubo, T.; Wada, K. *J. Catal.* **1994**, *148*, 138.

(19) Ushikubo, T.; Wada, K. *Appl. Catal., A* **1995**, *124*, 19.

(20) Guiu, G.; Grange, P. *J. Catal.* **1995**, *156*, 132.

(21) Van Der Voort, P.; Babitch, I. B.; Grobet, P. J.; Verberckmoes, A. A.; Vansant, E. F. *J. Chem. Soc., Faraday Trans.* **1996**, *92*, 3635.

(22) Baltes, M.; Van Der Voort, P.; Collart, O.; Vansant, E. F. *J. Porous Mater.* **1998**, *5*, 357.

(23) Baltes, M.; Collart, O.; Van Der Voort, P.; Vansant, E. F. *Langmuir* **1999**, *15*, 5841.

(24) Baltes, M.; Van Der Voort, P.; Weckhuysen, B. M.; Rao, R. R.; Catana, G.; Schoonheydt, R. A.; Vansant, E. F. *Phys. Chem. Chem. Phys.* **2000**, *2*, 2673.

(25) Baltes, M.; Cassiers, K.; Van Der Voort, P.; Weckhuysen, B. M.; Schoonheydt, R. A.; Vansant, E. F. *J. Catal.* **2001**, *197*, 160.

(26) Huuhtanen, J.; Sanati, M.; Andersson, A.; Andersson, S. L. T. *Appl. Catal A* **1993**, *97*, 197.

(27) Prinetto, F.; Ghiotto, G.; Occhiuzzi, M.; Indovina, V. *J. Phys. Chem. B* **1998**, *102*, 10316.

(28) Haukka, S.; Kytökivi, A.; Lakomaa, E.-L.; Lehtovirta, U.; Lindblad, M.; Lujala, V.; Suntola, T. In *Preparation of Catalysts VI, Scientific Bases for the Preparation of Heterogeneous Catalysts*; Poncelet, G., Ed.; p 957, Elsevier Science, Amsterdam, 1995; p 957.

(29) Kytökivi, A.; Lakomaa, E.-L.; Root, A.; Österholm, H.; Jacobs, J.-P.; Brongersma, H. H. *Langmuir* **1997**, *13*, 2717.

(30) Kytökivi, A.; Jacobs, J.-P.; Hakuli, A.; Meriläinen, J.; Brongersma, H. H. *J. Catal.* **1996**, *162*, 190.

(31) Schraml-Marth, M.; Wokaun, A.; Pohl, M.; Krauss, H. L. *J. Chem. Soc., Faraday Trans* **1991**, *87*, 2635.

(32) Scharf, U.; Schraml-Marth, M.; Wokaun, A.; Baiker, A. *J. Chem. Soc., Faraday Trans.* **1991**, *87*, 3299.

(33) Zhang, J.-Y.; Lim, B.; Boyd, I. W. *Thin Solid Films* **1998**, *336*, 340.

(34) Vuurman, M. A.; Stufkens, D. J.; Oskam, A.; Deo, G.; Wachs, I. E. *J. Chem. Soc., Faraday Trans.* **1996**, *92*, 3259.

(35) Ono, H.; Koyanagi, K. *Appl. Phys. Lett.* **2000**, *77*, 1431.

(36) Kantcheva, M. *Phys. Chem. Chem. Phys.* **2000**, *2*, 3043.

(37) Szanics, J.; Okubo, T.; Kakihana, M. *J. Alloy Compd.* **1998**, *281*, 206.

(38) Su, S. C.; Bell, A. T. *J. Phys. Chem.* **1998**, *102*, 7000.

(39) Sanati, M.; Andersson, A.; Wallenberg, L. R.; Rebenstorf, B. *Appl. Catal., A* **1993**, *106*, 51.

(40) Kataoka, T.; Dumesic, J. A. *J. Catal.* **1988**, *112*, 66.

(41) Rajagopal, S.; Marzari, J. A.; Miranda, R. *J. Catal.* **1995**, *151*, 192.

(42) Damyanova, S.; Grange, P.; Delmon, B. *J. Catal.* **1997**, *168*, 421.

(43) Tatibouët, J. M. *Appl. Catal., A* **1997**, *148*, 213.

(44) Forzatti, P.; Tronconi, E.; Elmi, A. S.; Busca, G. *Appl. Catal., A* **1997**, *157*, 387.

(45) Louis, C.; Tatibouët, J. M.; Che, M. *J. Catal.* **1988**, *109*, 354.

(46) Jehng, J.-M.; Hu, H.; Gao, X.; Wachs, I. E. *Catal. Today* **1996**, *28*, 335.

(47) Gao, X.; Bare, S. R.; Weckhuysen, B. M.; Wachs, I. E. *J. Phys. Chem. B* **1998**, *102*, 10842.

(48) Deo, G.; Wachs, I. E. *J. Catal.* **1994**, *146*, 323.

(49) Tanaka, T.; Nojima, H.; Yamamoto, T.; Takenaka, S.; Funabiki, T.; Yoshida, S. *Phys. Chem. Chem. Phys.* **1999**, *1*, 5235.

(50) Wachs, I. E.; Jehng, J.-M.; Deo, G.; Hu, H.; Arora, N. *Catal. Today* **1996**, *28*, 199.

(51) Vansant, E. F.; Van Der Voort, P.; Vrancken, K. C. *Characterization and Chemical Modification of the Silica Surface, Studies in Surface Science and Catalysis*; Elsevier: Amsterdam, 1995; Vol. 93.

(52) Peri, J. B. *J. Phys. Chem.* **1966**, *70*, 3168.

(53) Knözinger, H.; Ratnasamy, P. *Catal. Rev. Sci. Eng.* **1978**, *17*, 31.

(54) Clearfield, A.; Serette, G. P. D.; Khazi-Syed, A. H. *Catal. Today* **1994**, *20*, 295.